www.elsevier.com/locate/dsr2

Coastal barium cycling at the West Antarctic Peninsula

K.M. Pyle, K.R. Hendry, R.M. Sherrell, M.P. Meredith, H. Venables, M. Lagerström, A. Morte-Ródenas

PII: S0967-0645(16)30361-7
DOI: http://dx.doi.org/10.1016/j.dsr2.2016.11.010
Reference: DSRII4160

To appear in: *Deep-Sea Research Part II*

Cite this article as: K.M. Pyle, K.R. Hendry, R.M. Sherrell, M.P. Meredith, H Venables, M. Lagerström and A. Morte-Ródenas, Coastal barium cycling at the West Antarctic Peninsula, *Deep-Sea Research Part I* http://dx.doi.org/10.1016/j.dsr2.2016.11.010

Coastal barium cycling at the West Antarctic Peninsula

K.M. Pyle[a*], K.R. Hendry[b], R.M. Sherrell[c], M.P. Meredith[d], H. Venables[d], M. Lagerström[e], A. Morte-Ródenas[a]

[a] School of Earth and Ocean Sciences, Cardiff University, Main Building, Park Place, Cardiff, CF10 3AT

[b] School of Earth Sciences, University of Bristol, Wills Memorial Building, Queens Road, Bristol, BS8 1RJ

[c] Department of Marine and Coastal Sciences and Department of Earth and Planetary Sciences, Rutgers University, New Jersey, USA.

[d] British Antarctic Survey, High Cross, Madingley Road, Cambridge, CB3 0ET

[e] Department of Environmental Science and Analytical Chemistry (ACES), Stockholm University, SE-106 91 Stockholm, Sweden

Abstract

Barium cycling in the ocean is associated with a number of processes, including the production and recycling of organic matter, freshwater fluxes, and phenomena that affect alkalinity. As a result, the biogeochemical cycle of barium offers insights into past and present oceanic conditions, with barium currently used in various forms as a palaeoproxy for components of organic and inorganic carbon storage, and as a quasi-conservative water mass tracer. However, the nature of the oceanic barium cycle is not fully understood, particularly in cases where multiple processes may be interacting simultaneously with the dissolved and particulate barium pools. This is particularly the case in coastal polar regions such as the West Antarctic Peninsula, where biological drawdown and remineralisation occur in tandem with sea ice formation and melting, glacial meltwater input, and potential fluxes from shelf sediments.

Here, we use a high-precision dataset of dissolved barium (Ba_d) from a grid of stations adjacent to the West Antarctic Peninsula in conjunction with silicic acid ($Si(OH)_4$), the oxygen isotope composition of water, and salinity measurements, to determine the relative control of various coastal processes on the barium cycle throughout the water column. There is a strong correlation between Ba_d and $Si(OH)_4$ present in deeper samples, but nevertheless persists significantly in surface waters. This indicates that the link between biogenic opal and barium is not solely due to barite precipitation and dissolution at depth, but is supplemented by an association between Ba_d and diatom tests in surface waters, possibly due to barite formation within diatom-dominated phytodetritus present in the photic zone. Sea-ice meltwater appears to exert a significant secondary control on barium concentrations, likely due to non-conservative biotic or abiotic processes acting as a sink for Ba_d within the sea ice itself, or sea-ice meltwater stimulating non-siliceous productivity that acts as a Ba_d sink. Meteoric water input, conversely, exerts little or no control on

* *Corresponding author* PyleKM@cf.ac.uk

local barium levels, indicating that glacial meltwater is not a significant coastal source of barium to the West Antarctic Peninsula shelf waters.

Keywords: Barium; seawater; polar waters; trace metal; Antarctica; West Antarctic Peninsula; Pal LTER grid

1. Introduction

Records of dissolved and particulate barium (Ba) have been applied as proxies for several past and present oceanic variables and processes such as export production, alkalinity, and meltwater input (Hall and Chan, 2004; Jacquet et al., 2007; Lea and Boyle, 1989). The reliability of such proxies can be improved through an enhanced understanding of the oceanic Ba cycle. Current understanding of oceanic Ba dynamics is limited, particularly in regions where multiple factors may influence the dissolved barium pool.

Barium is a bio-intermediate element found in trace concentrations (30-160 nM) in the ocean (Chan et al., 1976; Dehairs et al., 1980; Wolgemuth and Broecker, 1970). Sourced from continental weathering, the main input of barium to the oceans is fluvial run-off (Guay and Falkner, 1998). A secondary source is dissolved barium from hydrothermal vent systems, which is thought to precipitate locally (Edmond et al., 1979; Von Damm et al., 1985).

Dissolved barium (Ba_d) in the ocean has a biointermediate nutrient-like distribution, with low concentrations at the surface that do not reach complete depletion, and increased concentrations at depth. A connection between surface water depletion of Ba_d and phytoplankton productivity has been established by numerous observations throughout the global ocean (Esser and Volpe, 2002; Hoppema et al., 2010; Nozaki et al., 2001), although the exact nature of this biologically-related uptake is yet to be established. Very few, if any, marine organisms actively take up barium directly (Bertram and Cowen, 1997; Griffith and Paytan, 2012). Whilst there is evidence for the presence of barium within phytoplankton (Ganeshram et al., 2003), either associated with organic material, incorporated into calcite ($CaCO_3$) or celestite ($SrSO_4$) tests (Bernstein and Byrne, 2004; Bernstein et al., 1992; Dymond and Collier, 1996; Lea and Spero, 1992), or adsorbed onto oxyhydroxides associated with opaline silica (Sternberg et al., 2005), the relative importance and viability of each of these associations is still under debate.

The involvement of barium in biological processes is reflected in its co-variance in global ocean waters with silicic acid and alkalinity (Dehairs et al., 1980; Lea and Boyle, 1989). An important factor in the nutrient-like behaviour of barium is thought to be the biologically-mediated nature of barium sulphate (barite) precipitation, which does not occur in bulk seawater because barite is undersaturated in most of the global ocean (Monnin and Cividini, 2006). It has been suggested that the formation of barite occurs by supersaturation resulting from elevated barium or sulphate within microenvironments created by decaying organic matter (Bishop, 1988; Dehairs et al., 1980). This causal link is supported by observations of the distribution of particulate barium in the water column (correlation with rates of oxygen consumption and

bacterial respiration (Dehairs et al. 1980; Bishop 1988; Jacquet et al. 2007; 2011; Thomas et al. 2011), association of barite crystals with bio-aggregates (Stroobants et al., 1991) and in sediments (correlation with organic carbon fluxes (Dymond and Collier, 1996; Dymond et al., 1992). The exact mechanism behind this precipitation, and the level of bacterial involvement, is still unclear (Gonzalez-Muñoz et al. 2012; Gonzalez-Muñoz et al. 2003).

As a result of its association with organic matter, biogenic barite has been established as a proxy for export productivity both in the modern ocean (Jacquet et al., 2007; Thomas et al., 2011) and in sediment cores representing past oceanic conditions (Nürnberg et al., 1994; Thompson and Schmitz, 1997). Records of the ambient marine concentration of dissolved barium (usually measured via the Ba/Ca ratio preserved in biogenic calcite or aragonite) can also yield pertinent information about past oceanic conditions, thanks to its co-variance with important parameters such as alkalinity, silicic acid, or riverine fluxes (Hall and Chan, 2004; LaVigne et al., 2016; Lea and Boyle, 1989; Plewa et al., 2006). However, the current limited understanding of the oceanic barium cycle can make it difficult to distinguish the influences of these various processes on the barium stocks of the water masses investigated.

Here, we investigate the controls on the distribution of dissolved barium in shelf-slope waters of the West Antarctic Peninsula (WAP), in order to improve our understanding of barium cycling in seawater and to improve the robustness of productivity proxy interpretations. Along the WAP, coastal processes such as sea ice formation and meltwater discharge can be observed alongside biological activity and ocean mixing, making it an ideal natural laboratory to study the relative controls that these processes exert on dissolved barium in seawater.

2. Materials and Methods

Seawater samples were collected from stations covering the Palmer Long Term Ecological Research (PalLTER) grid (Fig. 1) during annual cruises of the ARSV Lawrence M. Gould in two consecutive austral summers: LMG11-01 (2nd January 2011 – 6th February 2011) and LMG12-01 (30th December 2011 – 7th February 2012). Water was sampled either from surface water using a trace metal-clean towfish or at depth using Niskin bottles deployed on a CTD (Conductivity-Temperature-Depth) rosette. Dissolved barium concentration data reported here are publicly available within the PAL-LTER data system (dataset #266): http://oceaninformatics.ucsd.edu/datazoo/data/pallter/datasets.

2.1 Dissolved barium

The dissolved barium concentrations of 0.2 µm filtered (Acropak-200, Pall) seawater samples were analysed using isotope dilution inductively coupled plasma mass spectrometry (ID ICP-MS) (Klinkhammer and Chan, 1990). Samples were prepared for isotope dilution (ID) as follows: 250 µL aliquots of seawater were spiked gravimetrically with 200 µL of a ^{135}Ba-enriched solution (10 µg/mL ^{135}Ba, Inorganic Ventures,

Christiansburg, VA, USA, gravimetrically diluted to 0.013 µg/mL ^{135}Ba [96 nM] using high purity 3% HNO_3) to achieve a ^{138}Ba/^{135}Ba ratio of 0.7 - 1.0 to minimise error propagation (Klinkhammer and Chan, 1990). The concentration of the spike solution was calibrated via reverse isotope dilution using a commercial Ba natural standard solution from High-Purity Standards. Spiked solutions were then diluted 20 times with high purity 3% HNO_3 and homogenised.

Isotope ratios (^{138}Ba/^{135}Ba) were measured in spiked samples using a Thermo-Finnigan Element XR (Cardiff University) or Element-1 (Rutgers University) ICP-MS in low resolution mode, with dissolved barium concentrations subsequently calculated using Eq.1. A mass bias correction coefficient (K) was calculated each time samples were analysed by measuring the ratio of ^{138}Ba/^{135}Ba in a 1 ppb Ba natural standard solution prepared in 5% (v/v) seawater (NASS-6 seawater standard of 5 ppb ± 0.15 Ba), and comparing this to the average natural ratio reported in the literature (10.88) (Eq. 2). The isotope ratio determined in this solution varied between 10.5 and 11.1, with measured uncertainty across each sample run never exceeding 1.5% (2*RSD). This uncertainty was consistently less than the mass bias determined for each sample run, which was on average a 1.9% deviation from the literature value.

$$\mathrm{Conc_{sample}} = \mathrm{Conc_{spike}} \times \frac{\mathrm{m_{spike}}}{\mathrm{m_{sample}}} \times \left(\frac{\mathrm{R_{spike}} - \mathrm{KR_{sample}}}{\mathrm{KR_{sample}} - \mathrm{R_{natural\ standard}}}\right) \times \frac{\mathrm{f_{spike}}}{\mathrm{f_{natural\ standard}}} \quad (1)$$

Where: $\mathrm{Conc_{sample}}$ = concentration of barium in sample
$\mathrm{Conc_{spike}}$ = concentration of barium in spike
m = mass
R = ratio of ^{138}Ba/^{135}Ba in sample, spike, or natural standard
f = abundance of ^{135}Ba in spike or natural standard
K = mass bias correction coefficient for dilute seawater

$$\mathrm{K} = \left(\frac{\mathrm{R_{literature}}}{\mathrm{R_{dilute\ seawater}}}\right) \quad (2)$$

Blank solutions of 3% (v/v of concentrated reagent) HNO_3 in 18.2 MΩ·cm water were analysed to correct for background barium signal from the introduction system of the ICP-MS (^{135}Ba blank counts <0.1% of seawater sample counts; ^{138}Ba blank counts <1% of seawater sample counts), and a set of consistency standards were measured at regular intervals (see Table 1). A correction for any seawater matrix effects was applied to the blank measurements by monitoring the sensitivity of a natural standard solution in 3% HNO_3 vs. a natural standard solution in 5% seawater, before the blanks were subtracted from sample counts.

Sample preparation and measurements were split between the Department of Marine and Coastal Science at Rutgers University, NJ, and the School of Earth and Ocean Sciences at Cardiff University. At Rutgers a Thermo-Finnigan Element-1 (SEM detector only) was used for ICP-MS analysis, whilst at Cardiff an Element XR was used (dual mode SEM with Faraday detector), with the same counting mode method used

on both instruments. Seawater standards of comparable barium concentration to the samples show a long term external reproducibility of ±2% or better across all analytical runs at both facilities (2*RSD), and the same solutions measured repeatedly at both institutions show agreement within 1% (Table 1). Within each analytical run, reproducibility of these seawater standards was 1.1% or better. High precision analyses were necessary for discerning relatively subtle Ba gradients; the full range of Ba concentrations in this study is 70 - 105 nM, with the majority of data points falling at 78 - 85 nM.

2.2 Dissolved inorganic nutrients and primary productivity

Dissolved inorganic nutrients (silicic acid, phosphate, and nitrate plus nitrite) were analysed at the Marine Biological Laboratory (Woods Hole, MA) using a Lachat Quickchem 8000 nutrient analyser. The data are available at http://oceaninformatics.ucsd.edu/datazoo/data/pallter/datasets?action=summary&id=27 [†] (See Ducklow et al. (2013) and references therein for further information on the provenance of these datasets).

Direct quantification of primary productivity was calculated at a small number of sites in ^{14}C-labelled deck incubation experiments. Data and methodology overview are available at http://oceaninformatics.ucsd.edu/datazoo/data/pallter/datasets?action=summary&id=41#overview [‡] (Oscar Schofield).

2.3 Water mass fractions

Seawater samples were analysed for the ratio of stable oxygen isotopes at the Natural Environment Research Council Isotope Geosciences Laboratory (NIGL) at the British Geological Survey. Samples were equilibrated with CO_2 (Epstein and Mayeda, 1953) using a VG Isoprep 18, with $^{18}O/^{16}O$ ratios then measured on a SIRA 10 mass spectrometer. Results were reported in standard $\delta^{18}O$ notation, with reference to a standard (Vienna Standard Mean Ocean Water [VSMOW]).

At sample sites with measured values of salinity and $\delta^{18}O$, a three-end-member mass balance is used to derive the fractions of sea-ice melt, meteoric water, and Circumpolar Deep Water (CDW). This mass balance calculation is based on the de-coupled behaviour of salinity and $\delta^{18}O$ in the different freshwater sources: sea-ice melt, and freshwater of meteoric origin (glacial melt plus precipitation). Developed by Östlund & Hut (1984) for the Arctic, this mass balance (Eq. 3) is implemented at the West Antarctic Peninsula by Meredith et al. (2008, 2010, 2013, this issue).

$$f_{SI} + f_{MW} + f_{CDW} = 1$$
$$(S_{SI} * f_{SI}) + (S_{MW} * f_{MW}) + (S_{CDW} * f_{CDW}) = S \qquad (3)$$
$$(\delta_{SI} * f_{SI}) + (\delta_{MW} * f_{MW}) + (\delta_{CDW} * f_{CDW}) = \delta$$

[†] Accessed 22/10/2014
[‡] Accessed 13/10/2014

where f_{SI}, f_{MW}, and f_{CDW} are the fractions of sea-ice melt, meteoric water, and CDW, respectively, that we seek to determine; S_{SI}, S_{MW}, and S_{CDW} are the respective salinities of the end members; and δ_{SI}, δ_{MW}, and δ_{CDW} are their corresponding $\delta^{18}O$ values. The quantities S and δ are the measured values of salinity and $\delta^{18}O$ at the sample site. The salinity and $\delta^{18}O$ values assigned to each end member are: 34.73 and +0.1‰ for CDW; 7 and +2.1‰ for sea-ice melt; and 0 and -16‰ for meteoric water, respectively (Meredith et al. 2008; 2010; 2013). The resulting derived freshwater fractions are reported here as percentages: sea-ice melt fraction (%SI), and meteoric water fraction (%MW), with typical errors of <1% on point values (Meredith et al. 2013). The majority of this 1% error is due to uncertainty on the values attributed to end-members, and can therefore be considered to be systematic across the dataset.

The meteoric water fraction comprises freshwater input from glacial meltwater and from precipitation; quantitative separation of these components would require an additional conservative freshwater tracer to be measured, and such measurements are not available at this time. It should be noted, however, that the mean meteoric water budget at the WAP is believed to be dominated by glacial melt. This is consistent with rates of precipitation over the glacier catchments at the WAP being higher than mean rates of precipitation directly into the ocean, combined with the effect of the glaciers in delivering the accumulated freshwater directly into the ocean at the coast (Meredith et al. 2013). Whilst temporal variability in meteoric water may be influenced by changes in direct precipitation, the differences in precipitation over the relevant periods prior to the 2011 and 2012 years are small (Fig. 12 of Meredith et al., this issue).

3. Results

3.1 Distribution of dissolved barium

The spatial distribution of dissolved barium (Ba_d) in surface samples across the PalLTER grid shows similar patterns across the two years studied (Fig. 2). In both 2011 and 2012 concentrations of dissolved barium are higher on the shelf, dropping to lower levels at the majority of stations over the continental slope (bathymetric division of PalLTER stations between continental shelf and slope after Martinson et al. (2008)). The exceptions to this are stations over the slope in the southern lines of the grid (000 and -100 Lines), which show a continuation of the higher Ba_d concentrations observed on the shelf. This general pattern of distribution in the surface waters can also be observed in the silicic acid data (Fig. 2).

Despite these general similarities, there are distinct differences between the findings of the two years. Compared with the 2012 measurements, surface values of dissolved barium in 2011 are slightly but consistently elevated across the shelf, with particular highs in the area south-west of Marguerite Bay, and a distinctive low from the outer shelf across the shelf break in the northern peninsula region.

Two depth profiles from 2012 show the vertical distribution expected of a bio-intermediate element, with depleted surface values and enrichment at depth (Fig. 3). Concentrations of Ba_d are higher in the 500m water column at the 200.100 site (on the shelf) than corresponding depths at the 200.160 site (over the continental slope), though the profile follows a similar shape. Two samples taken within 70 m of the bottom at 200.100 are distinctly elevated relative to the rest of the profile. Below 1000m at the continental slope site, the water column is significantly enriched in Ba_d, exhibiting Ba_d concentrations approximately 5 nM higher than equivalent records of Ba_d concentrations measured in the Drake Passage in 2008 (Roeske and Rutgers van der Loeff, 2012) (Fig. 3a).

The changing Ba_d concentration from the open waters of the Drake Passage to the shelf waters of the PalLTER is examined by constructing an artificial section from the compilation of depth profiles from the Drake Passage (PS71/236 and PS71/230 from Polarstern cruise ANT-XXIV/3, Roeske and Rutgers van der Loeff, 2012) and LTER depth profiles (Sites 200.100 and 200.160), with the caveat that these profiles were collected in different years (2008 and 2012 respectively). Following the 34.7 isohaline along this section, Ba_d increases from approximately 82 nM at one of the open water sites (PS71/230) to approximately 88 nM on the slope (PalLTER station 200.160) and approximately 91 nM over the shelf (PalLTER station 200.100).

3.2 Inter-year variability in surface distribution

The inter-year variability observed is quantified by a simple calculation of the surface ΔBa_d (Ba_d^{2012} - Ba_d^{2011}) at each of the stations that were sampled in both years, along with the inter-year variability of other key parameters such as silicic acid and water mass fractions (denoted by Δ). The locations of underway stations were not identical between years, but were sufficiently close to warrant inclusion in this analysis.

There is a significant positive correlation between ΔBa_d and $\Delta Si(OH)_4$ (r^2=0.462; p=4.9*10^{-5}; $\Delta Si(OH)_4$ co-efficient=0.196; n=29), whilst a less distinct negative relationship is observed between ΔBa_d and the fraction of sea-ice melt present (Δ%SI) (r^2=0.316; p=0.0012; Δ%SI co-efficient=-1.75; n=30) (Fig. 4). No significant relationship is found between ΔBa_d and the inter-year variance of meteoric water input (Δ%MW) (r^2=0.016; p=0.49; Δ%MW co-efficient=0.709; n=30).

3.3 Dissolved barium and silicic acid

The full data set (2011 surface samples; 2012 depth and surface samples) shows a strong positive correlation between dissolved barium and silicic acid ($Si(OH)_4$) (Fig. 5), following a linear regression model similar to that observed elsewhere in the Southern Ocean and adjoining basins (Table 2), but with a lower slope coefficient and a higher intercept at zero $Si(OH)_4$. In the case of the PalLTER dataset this regression is heavily reliant on the relatively few depth values available, although a significant yet more scattered positive relationship still exists when surface samples are considered independently (Table 2). When dissolved barium values are normalised to an average salinity (33.5) a small component of this coupled variation is removed, but the relationship remains significant.

A large amount of scatter exists around this $Ba_d/Si(OH)_4$ relationship, which is examined through the calculation of a $Ba_{Si}^{Residual}$ value for each data point. The $Ba_{Si}^{Residual}$ value quantifies the deviation of the Ba_d measurement from the overall $Ba_d/Si(OH)_4$ regression of the dataset (Eq. 4). Positive $Ba_{Si}^{Residual}$ values indicate that the Ba_d measured is higher than predicted by silicic acid values, whilst negative $Ba_{Si}^{Residual}$ values signify that Ba_d is lower than predicted.

$$Ba_{Si}^{Residual} = Ba_d^{Measured} - ((Si(OH)_4^{Measured} * 0.21) + 69.2)) \quad (4)$$

Surface plots of these $Ba_{Si}^{Residual}$ values identify several areas of interest (Fig. 2). In the 2011 plot the area adjacent to and southwest of Marguerite Bay is highlighted by very high values, corresponding to an anomalous pairing of high Ba_d relative to $Si(OH)_4$ measurements in this region. The 2012 plot reveals lower $Ba_{Si}^{Residual}$ values overall, but with significant lows around Marguerite Bay and at certain points along the coast (400 and 600 line transects).

3.4 Productivity indicators

Primary productivity in this region is considered to be dominated by diatoms (Ducklow et al., 2007). As diatoms are siliceous organisms it is common to consider levels of silicic acid in surface waters as representative of the relative abundance of diatom populations across an area. Higher levels of surface silicic acid may result from low uptake, indicating lower levels of diatom productivity, and vice versa. However, in the 2011 and 2012 surface datasets from this area there is no significant correlation between silicic acid and primary productivity (R^2=0.01; p=0.54; n=35), or silicic acid and Chl-a (R^2=0.01; p=0.52; n=44). This suggests that surface silicic acid levels may not be a suitable indicator of diatom productivity, or that non-siliceous forms of productivity were dominant at this time. Both measured primary productivity in surface waters (R^2=0.30/0.27; p<0.01; n=30) and Chl-a (R^2=0.22/0.46; p<0.01; n=40) exhibit significant negative correlations with other macronutrients (phosphate; nitrate plus nitrite respectively).

3.5 Dissolved barium and water mass fractions

As well as significant variation in the dissolved barium distribution, the two years studied exhibit very different regimes of freshwater input (Fig. 6). The 2012 data are dominated by a higher sea-ice melt input, focussed in the region adjacent to and southwest of Marguerite Bay, and at certain sites along the coast to the northeast (400 and 600 Lines). Variations in the meteoric water contribution reveal a contrast between gentle gradients perpendicular to the coast in the 2012 data, and localised areas of higher meteoric water concentrations in 2011. Given the general similarity of precipitation inputs preceding the cruises in these two years (Meredith et al., this issue), the differences are most likely due to localised changes in glacier discharge, though some impact of precipitation changes cannot be excluded.

The behaviour of the Ba_d distribution in relation to salinity also differs between the two years, indicating that variation in Ba_d is not merely a feature of ion concentration or dilution (i.e. not a result of conservative processes). A large portion of the data for 2011 and 2012 define a similar trend of varying Ba_d values over a narrow range or salinity, which is relatively high for the location. A subset of both datasets then deviate from this main trend; in 2011 sample sites close to the coast record constant Ba_d values as salinity decreases, in 2012 a larger subset (defined by sample sites in Marguerite Bay and the southwest, and those close to the coast) record Ba_d values decreasing slightly with salinity (Fig. 7).

Linear regression modelling between the derived meteoric water fraction (%MW) and Ba_d indicates that %MW is significantly correlated with Ba_d, particularly for the 2011 sample set (2011 data: r^2=0.23, p=0.0017, %MW co-efficient=2.29, n=41; 2012 data: r^2=0.097; p=0.024; %MW co-efficient=1.19; n=52). However, this correlation appears to be an artefact produced by two subsets of data, with most off-shelf sites having consistently low Ba_d and %MW, whilst on-shelf sites exhibit a variation in %MW that is not accompanied by any predictable change in Ba_d (Fig. 8). Off-shelf sites from the southern lines of the grid (000 and -100 Lines) in 2012 also exhibit this broadly shelf-like behaviour.

In the 2012 data, areas of low $Ba_{Si}^{Residual}$ values (around Marguerite Bay and at certain points along the coast) appear to correspond with sites of high sea-ice melt input. These observations are corroborated by the appearance of a slight negative correlation between 2012 $Ba_{Si}^{Residual}$ values and the contribution of sea-ice melt (r^2=0.24, p<0.01, %SI co-efficient=-0.92, n=52) (Fig. 9a).

3.6 Vertical mixing

The extent to which upper-ocean vertical mixing has affected the water column at the stations is very difficult to quantify directly, although systematic collection of the necessary measurements has been initiated for the WAP (Brearley et al., this issue). In the absence of these mixing data, the impact of mixing on the structure of the water column can be estimated by calculating the mixed layer depth, defined here as the depth at which the potential density anomaly of the water column exceeds 0.05 kg m^{-3} of the surface value (Clarke et al., 2008). An alternative way to quantify the degree of water column stratification is to calculate the density difference between several different depth ranges (Hendry et al., 2010). Whilst the former method provides an upper limit to the current depth to which the ocean is actively mixing, the latter represents the strength of the stratification present in the ocean, which at the WAP is known to be influenced by the level of upper-ocean homogenisation the previous winter (Venables et al., 2013). Estimates of stratification from both of these methods were compared to silicic acid and dissolved barium distribution across the LTER grid, and show no significant correlation.

4. Discussion

4.1 Biological cycling as a primary control on the surface dissolved barium distribution

Although mainly dominated by diatoms and cryptophytes, the phytoplankton assemblage of the WAP has been shown to display complex spatial and temporal variations, with regional contributions from haptophytes and flagellates (Huang et al., 2012). However, studies of phytoplankton community structure at the LTER have consistently reported high abundances of diatoms and cryptophytes relative to other groups, with diatoms dominating most of the offshore, southern coast and southern shelf areas (Garibotti et al., 2003; Huang et al., 2012; Kozlowski et al., 2011; Moline et al., 2004). It is therefore reasonable to assume that any biologically mediated removal of barium from surface waters in this region would be influenced by diatom productivity, and that silica cycling may play an important role in controlling Ba_d in the water column.

In accord with previous observations, the Ba_d distribution across the PalLTER grid co-varies with silicic acid concentrations (Fig. 2). A strong positive correlation (r^2=0.71; $p<0.01$ [significance is considered throughout at 99% confidence limits]; Fig. 5) between Ba_d and $Si(OH)_4$ is observed when samples from the whole water column are considered, with much of the relationship defined by a limited number of samples from intermediate and deeper waters. This agrees with previous suggestions that the strong association between barium and silicic acid is sustained by samples at depth. These distributions may result from a similarity in inorganic dissolution behaviour between biogenic opal and barium, coupled with large scale ocean circulation (Horner et al., 2015; Jacquet et al., 2007; Jeandel et al., 1996). However, direct links have been suggested between the marine silicic acid and barite cycles, with studies in the Southern Ocean reporting higher levels of barite particulates observed in diatom-dominated regions, potentially due to the catalytic effects of sinking diatom frustules on barite precipitation (Bishop, 1988; Dehairs et al., 1991; Stroobants et al., 1991).

The overall Ba_d-$Si(OH)_4$ relationship in this region is defined by the depth samples, whilst the surface sites that comprise the majority of the dataset display a lower degree of variability in both Ba_d and $Si(OH)_4$ distribution. However, the relationship between the two parameters does not de-couple entirely in surface waters as has been observed in other regions of the Southern Ocean (Jacquet et al., 2007). Considered independently of the depth profiles, the surface PalLTER dataset still displays a significant, though highly scattered, positive correlation (r^2=0.27; $p<0.01$; see Table 2) between Ba_d and $Si(OH)_4$ (Fig. 5). Conversely, surface Ba_d shows no significant correlation with the other macronutrients nitrate and phosphate. This indicates that the association between Ba_d and $Si(OH)_4$ in surface waters is not related directly to biological uptake or the cycling of organic material. Whilst the high level of interannual variability in the surface Ba_d distribution can be largely accounted for by variability in surface concentrations of $Si(OH)_4$ (Fig. 4a), this variability does not seem to be linked to estimates of primary productivity, but instead may indicate the varying balance between the removal of $Si(OH)_4$ from surface water via sinking biogenic opal, and recycling

between biogenic opal and $Si(OH)_4$ in surface waters. Low concentrations of surface $Si(OH)_4$ may reflect a local dominance of sinking over surface recycling, possibly due to the formation of heavier diatom tests in response to iron limitation (Hutchins and Bruland, 1998; Timmermans and van der Wagt, 2010).

It is possible that, rather than silicic acid concentrations indicating increased diatom productivity or export, the covariance of silicic acid and dissolved barium could result instead from a coincident replenishment of surface stocks via upwelling. However, the lack of correlation between the surface variability of these parameters and estimates of water column stratification (mixed layer depths and density differences, see Section 3.6) make such a scenario unlikely in this case, as any increased vertical mixing in the vicinity of these higher surface concentrations should be detectable using such methods. It is likely that vertical mixing does play a role in Ba_d cycling, but long-term mixing rates are not currently well-constrained by observations except in a few specific locations (such as the Rothera Oceanographic and Biological Time Series site [RaTS] Brearley et al., this issue).

In addition to the association between Ba_d and $Si(OH)_4$, there is a notable lack of correlation between $Si(OH)_4$ and the other macronutrients in surface waters (phosphate: r^2=0.25; p=0.023. nitrate plus nitrite: r^2=0.03; p=0.79). This could result from relatively shallow remineralisation of phosphate and nitrate, allowing them to be mixed back into the surface layer. Whilst a large proportion of biogenic opal is recycled in surface waters (>50% in the Southern Ocean (Tréguer and De La Rocha, 2013)), the exported fraction dissolves deeper in the water column. Whilst the association between Ba_d and silicic acid at depth is well established, the association observed here in surface waters, albeit weaker, suggests that in this diatom-dominated region, the phase carrying Ba_d from surface waters to the mesopelgic depths of barite precipitation is associated with silicic diatom frustules rather than with organic matter. Ba_d has been found to associate with iron oxyhydroxides adsorbed onto diatom cell surfaces is laboratory cultures (Sternberg et al., 2005), which could cause the surface correlation observed if this occurred on a large scale. However, no significant levels of iron have been found on the surfaces of Southern Ocean phytoplankton cells (Twining and Baines, 2013), making it unlikely that such a mechanism could have a large impact on Ba_d distributions. It is more likely that Ba_d is associated with biogenic opal-dominated phytodetritus within the euphotic layer through barite precipitation (Horner et al., 2015) that may be catalysed by the presence of diatom frustules (Bishop, 1988; Stroobants et al., 1991). This would explain the positive correlation observed between Ba_d and $Si(OH)_4$ in surface waters, with low concentrations of both occurring when the sinking and export of biogenic opal dominates over surface recycling, providing within its phytodetrital microenvironments conditions for the precipitation of barite.

The lower slope and higher intercept value of the surface Ba_d-$Si(OH)_4$ linear regression model implies that in surface waters Ba_d is less variable in relation to silicic acid than it is in deeper waters, with the processes that govern Ba_d distributions differing between surface waters and the deeper water column.

There are several mechanisms that could explain this deviation by altering the ratio of Ba:Si in surface waters, such as differences in phytoplankton ecology (varying the extent to which Ba_d and/or silicic acid are removed from the surface), or additional abiotic processes leading to variation in the Ba:Si removal ratio. Processes may also be at work that alter the Ba:Si ratio in deeper waters that are relatively isolated from the surface, such as differences in the saturation state of the water column with regards to barite (influencing the regeneration ratio of Ba:Si), or variation in epibenthic fluxes. Different combinations of these mechanisms have been employed by previous authors to explain the geographical variation observed in the Ba_d-$Si(OH)_4$ relationship (Hoppema et al., 2010; Jacquet et al., 2007; Jeandel et al., 1996). The high density spatial coverage and biogeochemical gradients of the PalLTER dataset makes it ideal for testing the potential additional controls on surface uptake.

4.2 Identifying a coastal source of dissolved barium

As well as variation in surface uptake, the distribution of Ba_d will be influenced by any local changes to the sources of barium along the peninsula. Therefore it is necessary to assess through which processes barium is transported into the WAP coastal system. The general distribution of surface Ba_d (Fig. 2) indicates a coastal source that enriches waters on the shelf, with concentrations decreasing away from the coast as shelf waters mix with the Ba_d-poor waters of the Antarctic Circumpolar Current. In near-continent settings elsewhere this coastal enrichment could be attributed to fluvial input. The bulk of the barium weathered from continental rock is transported fluvially in the dissolved phase, causing the high surface concentrations of Ba_d routinely recorded at river mouths (Martin and Meybeck, 1979; Viers et al., 2009). The levels of Ba_d in these regions are increased by estuarine desorption of barium from river-borne sediments in the river/ocean mixing zone (Guay and Falkner, 1998; Hanor and Chan, 1977; Nozaki et al., 2001).

However, along the coast of the WAP continental freshwater input is restricted to glacial meltwater and precipitation, which plays an important role in the physical and biological dynamics of the water column. As well as releasing low salinity water to the coastal system, meltwater from glaciers may be enriched in terrigenous material acquired through contact with bedrock and dust accumulation (Raiswell et al., 2008; Sherrell et al., 2015). The input of this terrigenous material to marine waters can affect turbidity and light attenuation (Schloss et al., 2002), as well as being a potential source of macro and micronutrients. Differences in the presence of surface meltwater have been linked to variations in phytoplankton biomass both near- and offshore, probably as a result of water column stabilisation (Dierssen et al., 2002). Increased productivity has been observed surrounding free-drifting icebergs in the Weddell Sea in conjunction with evidence for the dispersion of entrained terrigenous particles (Smith et al., 2007) suggesting that glacial ice may also provide a source of trace metals that can stimulate primary production. Studies in Marian Cove (King George Island) have also shown that melting glaciers can be responsible for enriching coastal waters with macronutrients, trace elements, and rare earth elements (Kim et al., 2015).

Specific data regarding the barium content of glacial meltwater are sparse, and studies have shown that the solute and particulate composition of such waters can be highly variable (Mora et al., 1994). Attempts to characterise the trace element export of alpine glaciers have found that in these environments barium is present in significantly lower concentrations than in global stream waters (bulk glacial meltwater in the region of 5 nM Ba_d; average world stream water in the region of 145 nM Ba_d) (Fortner et al., 2009; Mitchell et al., 2001). This Fig. is also significantly lower than surface coastal Ba_d values reported from this study (70 - 85 nM), so if the content of WAP glacial meltwater is comparable then it may act to dilute local Ba_d concentrations rather than enriching them. Given the relatively high load of suspended sediment transported in glacial meltwater, it is possible that this could include a high concentration of adsorbed barium. However, this would be expected to desorb into the dissolved pool fairly quickly upon mixing with seawater, as is seen in desorption of barium from riverine sediment loads in estuaries, which we do not observe.

The data from the PalLTER show a significant, though highly scattered, positive trend between the derived meteoric water fraction (%MW) and Ba_d for both of the years studied (Fig. 8). However, these trends appear to be an artefact of two spatial subsets within the data: off-shelf sites with a low meteoric water component and low Ba_d values, and on-shelf sites where Ba_d variation is not linked to %MW. This interpretation is further supported by the lack of a consistent co-variance between Ba_d and salinity (Fig. 7) indicating that trace element input from glacial meltwater is not responsible for the Ba_d enrichment observed in the WAP shelf waters. There is some indication from surface distributions that areas with pronounced glacial meltwater input in 2011 may be associated with anomalously high Ba_d measurements (Fig. 2 and Fig. 6). It is possible that when fluxes of meltwater are sufficiently high, they may lead to localised Ba_d enrichment.

Previous studies of the distribution of marine Ba_d have reported significant barium enrichment in bottom waters, potentially a result of recycling of particulate barium phases from pelagic sediment (Hoppema et al., 2010; Jacquet et al., 2004). Barium is delivered to the sediment in various reactive forms: as particulate barium sulphate (barite), incorporated in celestite or calcite tests, and adsorbed onto Fe-Mn oxyhydroxides and organic matter. The release of Ba^{2+} from these solid phases during early diagenesis can saturate pore waters with respect to barium sulphate, creating a sharp concentration gradient at the sediment/seawater interface. This could lead to a diffusive flux of Ba_d to the overlying water column. There is evidence for such epibenthic Ba_d fluxes in pore water profiles from the Arabian Sea and the Equatorial Pacific (Paytan and Kastner, 1996; Schenau et al., 2001), and benthic incubation experiments that have directly measured barium fluxes from sediments (McManus et al., 1998, 1994). The existence of comparable Ba_d fluxes from the shelf sediments adjacent to the WAP could be responsible for observed enrichment of the overlying shelf waters. However, this hypothesis is difficult to test conclusively without more extensive

sampling of shelf bottom waters. The apparent increase of Ba_d concentrations observed along isopycnals from the open waters of the Drake Passage to the slope and shelf waters of the WAP indicates that Ba_d addition is taking place on the shelf. However, as these Ba_d records were not collected in the same year, this comparison is not conclusive. The dissolution of particulate barium phases within shelf sediments could lead to a flux of barium from the sediment to bottom waters on the shelf. These fluxes are a plausible source of barium to coastal waters, and could be responsible for the observed Ba_d-$Si(OH)_4$ relationship if both silicic acid and barium were diffusing from benthic sources with a relatively low Ba:Si ratio, lowering the regression slope relative to other regions of the ocean whilst still enriching shelf waters with Ba_d.

4.3 Sea ice formation as a secondary control on the surface dissolved barium distribution

As discussed above, the observed correlation between barium and silicic acid is not consistent throughout the water column, breaking down to some degree in surface waters. Additional abiotic factors must exist that influence variation in the uptake ratio of barium to silicic acid or the saturation state of barite in the water column. It is possible to investigate such abiotic processes, and how they may exert a secondary influence on the surface Ba_d distribution, by using $Ba_{Si}^{residual}$ values (see Section 3). Likely candidates to cause variation in the Ba_d concentration unrelated to biological productivity are the spatial and interannual variations in the coastal freshwater regime. As discussed in section 4.1, the meteoric water fraction (%MW) appears to have little impact on Ba_d distributions spatially in either 2011 or 2012. This is borne out by a lack of any significant co-variance between %MW and $Ba_{Si}^{Residual}$ values (2011 surface dataset: r^2=0.079; p=0.079; n=40. 2012 surface dataset: r^2=0.028; p=0.233; n=52).

In contrast, the fraction of sea-ice melt (%SI) present at sites in 2012 exhibits a significant negative correlation with $Ba_{Si}^{residual}$ values (r^2=0.235; p=0.00026; SI% co-efficient=-0.92; n=52) (Fig. 9a), suggesting that higher fractions of sea-ice melt are associated with lower dissolved barium concentrations than predicted by silicic acid levels, and vice versa. The surface plots of %SI and $Ba_{Si}^{residual}$ (Fig. 2 and Fig. 6) reveal that in 2012 the high %SI values recorded around Marguerite Bay and the southwest section of the PalLTER grid, plus at the coastal sites of the 400 and 600 lines, correspond to similarly distributed low $Ba_{Si}^{residual}$ values. A correlation with anomalously low barium concentrations suggests that fluxes of sea-ice melt to surface coastal waters dilute the stock of Ba_d present to a greater degree that they dilute the silicic acid stocks.

The concentrations of Ba_d found in sea ice (10 - 40 nM (Lannuzel et al., 2011)) are significantly lower than the seawater values reported here, so some degree of dilution would be expected from mixing with sea-ice meltwater. However, the disproportionate dilution of Ba_d relative to silicic acid suggests that there may be processes occurring within the sea ice that remove Ba_d, causing resultant meltwater to have a lower Ba:Si ratio than the seawater it formed from.

This dilution signal can be seen in a significant though highly-scattered positive correlation between the 2012 $Ba_{Si}^{residual}$ values and salinity (r^2=0.154; p=0.004; n=51) (Fig. 9b). Assuming the $Ba_{Si}^{residual}$ values to be

due to changing concentrations of Ba_d only, the slope of this relationship (1.92) represents an approximately 2.4% change in Ba_d for a 3% change in salinity, indicating that this Ba_d depletion is a pure dilution signal rather than a result of non-siliceous productivity stimulated by the sea-ice melt. Mechanisms such as abiotic barite precipitation in supersaturated brine channels, adsorption onto sea-ice algal cells, or biotic precipitation of barite associated with the degradation of algal communities within sea ice, have been proposed as potential pathways linking the presence of sea ice with observed barium depletion in polar surface waters (Falkner et al., 1994; Hoppema et al., 2010). Carson (2008) found that dissolved barium concentrations in sea ice brines from Adelaide Island (WAP) ranged widely from surface water concentrations, and preliminary work on further samples from the same site show Ba_d exhibiting variation along salinity gradients that is distinct from its behaviour in seawater (Pyle et al., unpublished). Sea ice has been found to contain high levels of particulate barium (up to 3000 pM in East Antarctic pack and fast ice (Lannuzel et al., 2011) and 7000 pM in Scotia Sea brown ice (Stroobants et al., 1991)), which supports the possibility that high levels of barite precipitation may be occurring within sea ice, removing barium from solution.

There is no indication of a similar relationship in the 2011 data, possibly because of a lower flux of sea-ice melt in this year. The average contribution of sea-ice melt to sample sites (%SI) was an order of magnitude lower in 2011 (0.085%) than in 2012 (0.56%), with the difference even more apparent in coastal/shelf sites (0.035% in 2011, 0.56% in 2012). The freshwater regime in 2011 was dominated by meteoric water fluxes, which appear to have a negligible influence on barium distributions. In order to test this idea, multiple regression analysis was performed using the independent variables of interyear variance in $Si(OH)_4$, %SI and %MW to determine the dependent variable ΔBa_d. As can be seen in Table 3, both $\Delta Si(OH)_4$ and Δ%SI were shown to be significant predictors, whilst Δ%MW has no significant effect.

5. Conclusions

This high resolution dataset of the distribution of dissolved barium across the PalLTER grid shows that there is a clear relationship between dissolved barium and silicic acid in the water column studied. This relationship is robust not only with depth, but also across the surface waters of the PalLTER grid, and the high level of inter-year variability exhibited by the Ba_d distribution between 2011 and 2012 correlates with the high inter-year variability of silicic acid concentrations. The persistence of the $Ba_d/Si(OH)_4$ relationship in these diatom-dominated surface waters is in contrast to the total breakdown of the relationship observed in other regions. It is possible that the removal of Ba_d from surface waters is facilitated by the presence of diatoms, either by adsorption of Ba_d onto particulates associated with diatoms, or via barite precipitation within diatom-dominated phytodetritus in the euphotic zone. Higher levels of biogenic opal export from surface waters (relative to recycling within the mixed layer) therefore lowers both surface silicic acid

concentrations and Ba_d concentrations, adding another dimension to the link between barium and silicic acid cycling.

Our new data also reveal that a coastal source of barium enriches the shelf waters before they mix with barium-depleted ACC waters at the shelf break. This coastal flux of barium is not attributed to glacial meltwater input, which appears to have no consistent impact on the dissolved barium distribution. The enrichment of shelf waters may be due to an epibenthic flux of barium from shelf sediments, but further investigation of sediment pore waters and depth profiles will be necessary to establish this.

Non-conservative processes acting during the formation of sea ice also act as a secondary control on the removal of barium from the surface layer. When high levels of sea-ice melt dominate the freshwater regime of the coastal waters of the WAP, local surface concentrations of dissolved barium are significantly lowered.

Acknowledgements

This work has been funded by NERC studentship 126577 and EU FP7_PEOPLE-20120CIG Proposal number 320070. We would like to thank the captain and crew of the ARSV Lawrence M. Gould, Marie Seguret for collecting seawater samples, and Hugh Ducklow and all other contributors to the Palmer, Antarctica Long Term Ecological Research Project, funded by NSF Awards-ANT 0823101 and PLR 1440435. We are grateful to members of the Bristol Oceans Past and Present (BOPP) Research Group at the University of Bristol, and Dr Carrie Lear and Professor Ian Hall at Cardiff University for insightful and constructive discussion of the data. Thanks also to the Editor Dr. Jacqueline Stefels and two anonymous reviewers for significantly improving the manuscript.

6. References

Bernstein, R.E., Byrne, R.H., 2004. Acantharians and marine barite. Mar. Chem. 86, 45–50. doi:10.1016/j.marchem.2003.12.003

Bernstein, R.E., Byrne, R.H., Betzer, P.R., Greco, A.M., 1992. Morphologies and transformations of celestite in seawater: The role of acantharians in strontium and barium geochemistry. Geochim. Cosmochim. Acta 56, 3273–3279. doi:10.1016/0016-7037(92)90304-2

Bertram, M. a., Cowen, J.P., 1997. Morphological and compositional evidence for biotic precipitation of marine barite. J. Mar. Res. 55, 577–593. doi:10.1357/0022240973224292

Bishop, J.K.B., 1988. The barite-opal-organic carbon association in oceanic particulate matter. Nature. doi:10.1038/332341a0

Brearley A. J., Meredith M. P., Naveira-Garabato A. C., Venables H. J. and Inall M. E. (2016) Controls on turbulent mixing processes on the West Antarctic Peninsula Shelf. Deep. Res. Part II Top. Stud. Oceanogr. (in press).

Carson, D.S., 2008. Biogeochemical Controls on Productivity and Particle Flux in the Coastal Antarctic Sea Ice Environment. PhD Thesis Submitt. Sch. Geosci. Fac. Sci. Eng. Edinburgh Univ.

Chan, L.H., Edmond, J.M., Stallard, R.F., Broecker, W.S., Chung, Y.C., Weiss, R.F., Ku, T.L., 1976. Radium and barium at GEOSECS stations in the Atlantic and Pacific. Earth Planet. Sci. Lett. 32, 258–267.

Clarke, A., Meredith, M.P., Wallace, M.I., Brandon, M.A., Thomas, D.N., 2008. Seasonal and interannual variability in temperature, chlorophyll and macronutrients in northern Marguerite Bay, Antarctica. Deep. Res. Part II Top. Stud. Oceanogr. 55, 1988–2006.

Dehairs, F., Chesselet, R., Jedwab, J., 1980. Discrete suspended particles of barite and the barium cycle in the open ocean. Earth Planet. Sci. Lett. 49, 528–550.

Dehairs, F., Stroobants, N., Goeyens, L., 1991. Suspended barite as a tracer of biological activity in the Southern Ocean. Mar. Chem. 35, 399–410. doi:10.1016/S0304-4203(09)90032-9

Dierssen, H.M., Smith, R.C., Vernet, M., 2002. Glacial meltwater dynamics in coastal waters west of the Antarctic peninsula. Proc. Natl. Acad. Sci. U. S. A. 99, 1790–1795. doi:DOI 10.1073/pnas.032206999

Ducklow, H., Fraser, W., Meredith, M., Stammerjohn, S., Doney, S., Martinson, D., Sailley, S., Schofield, O., Steinberg, D., Venables, H., Amsler, C., 2013. West Antarctic Peninsula: An Ice-Dependent Coastal Marine Ecosystem in Transition. Oceanography 26, 190–203. doi:10.5670/oceanog.2013.62

Ducklow, H.W., Baker, K., Martinson, D.G., Quetin, L.B., Ross, R.M., Smith, R.C., Stammerjohn, S.E., Vernet, M., Fraser, W., 2007. Marine pelagic ecosystems: the West Antarctic Peninsula. Philos. Trans. R. Soc. B Biol. Sci. 362, 67–94. doi:10.1098/rstb.2006.1955

Dymond, J., Collier, R., 1996. Particulate barium fluxes and their relationships to biological productivity. Deep Sea Res. Part II Top. Stud. Oceanogr. 43, 1283–1308. doi:10.1016/0967-0645(96)00011-2

Dymond, J., Seuss, E., Lyle, M., 1992. Barium in deep-sea sediment: A geochemical proxy for paleoproductivity. Paleoceanography 7, 163–181.

Edmond, J.M., Measures, C., McDuff, R.E., Chan, L.H., Collier, R., Grant, B., Gordon, L.I., Corliss, J.B., 1979. Ridge crest hydrothermal activity and the balances of the major and minor elements in the ocean: The Galapagos data. Earth Planet. Sci. Lett. 46, 1–18. doi:10.1016/0012-821X(79)90061-X

Epstein, S., Mayeda, T., 1953. VARIATION OF O-18 CONTENT OF WATERS FROM NATURAL SOURCES. Geochim. Cosmochim. Acta 4, 213–224. doi:10.1016/0016-7037(53)90051-9

Esser, B.K., Volpe, A.M., 2002. At-sea high-resolution chemical mapping: Extreme barium depletion in North Pacific surface water. Mar. Chem. 79, 67–79. doi:10.1016/S0304-4203(02)00037-3

Falkner, K.K., Macdnald, R.., Carmack, E.., Weigarter, T., 1994. The Potential of Barium as a Tracer of Arctic Water Masses. Polar Ocean. Their Role Shap. Glob. Environ. Geophys. Monogr. 85, 63–76.

Fortner, S.K., Lyons, W.B., Fountain, A.G., Welch, K.A., Kehrwald, N.M., 2009. Trace element and major ion concentrations and dynamics in glacier snow and melt: Eliot Glacier, Oregon Cascades. Hydrol. Process.

23, 2987–2996.

Ganeshram, R.S., François, R., Commeau, J., Brown-Leger, S.L., 2003. An experimental investigation of barite formation in seawater. Geochim. Cosmochim. Acta 67, 2599–2605. doi:10.1016/S0016-7037(03)00164-9

Garibotti, I., Vernet, M., Ferrario, M., Smith, R., Ross, R., Quetin, L., 2003. Phytoplankton spatial distribution patterns along the western Antarctic Peninsula (Southern Ocean). Mar. Ecol. Prog. Ser. 261, 21–39. doi:10.3354/meps261021

Gonzalez-Muñoz, M.T., Fernandez-Luque, B., Martinez-Ruiz, F., Ben Chekroun, K., Arias, J.M., Rodriguez-Gallego, M., Martinez-Canamero, M., de Linares, C., Paytan, A., 2003. Precipitation of barite by Myxococcus xanthus: possible implications for the biogeochemical cycle of barium. Appl Env. Microbiol 69, 5722–5725. doi:10.1128/aem.69.9.5722-5725.2003

Gonzalez-Muñoz, M.T., Martinez-Ruiz, F., Morcillo, F., Martin-Ramos, J.D., Paytan, a., 2012. Precipitation of barite by marine bacteria: A possible mechanism for marine barite formation. Geology 40, 675–678. doi:10.1130/G33006.1

Griffith, E.M., Paytan, A., 2012. Barite in the ocean - occurrence, geochemistry and palaeoceanographic applications. Sedimentology 59, 1817–1835. doi:10.1111/j.1365-3091.2012.01327.x

Guay, C.K., Falkner, K.K., 1998. A survey of dissolved barium in the estuaries of major Arctic rivers and adjacent seas. Cont. Shelf Res. 18, 859–882. doi:10.1016/S0278-4343(98)00023-5

Hall, J.M., Chan, L.-H., 2004. Ba/Ca in Neogloboquadrina pachyderma as an indicator of deglacial meltwater discharge into the western Arctic Ocean. Paleoceanography 19, 1–9. doi:10.1029/2003PA000910

Hanor, J.S., Chan, L.-H., 1977. Non-conservative behavior of barium during mixing of Mississippi River and Gulf of Mexico waters. Earth Planet. Sci. Lett. 37, 242–250. doi:10.1016/0012-821X(77)90169-8

Hendry, K.R., Meredith, M.P., Measures, C.I., Carson, D.S., Rickaby, R.E.M., 2010. The role of sea ice formation in cycling of aluminium in northern Marguerite Bay, Antarctica. Estuar. Coast. Shelf Sci. 87, 103–112. doi:10.1016/j.ecss.2009.12.017

Hoppema, M., Dehairs, F., Navez, J., Monnin, C., Jeandel, C., Fahrbach, E., de Baar, H.J.W., 2010. Distribution of barium in the Weddell Gyre: Impact of circulation and biogeochemical processes. Mar. Chem. 122, 118–129. doi:10.1016/j.marchem.2010.07.005

Horner, T.J., Kinsley, C.W., Nielsen, S.G., 2015. Barium-isotopic fractionation in seawater mediated by barite cycling and oceanic circulation. Earth Planet. Sci. Lett. 430, 511–522.

Huang, K., Ducklow, H., Vernet, M., Cassar, N., Bender, M.L., 2012. Export production and its regulating factors in the West Antarctica Peninsula region of the Southern Ocean. Global Biogeochem. Cycles 26.

Hutchins, D. a, Bruland, K.W., 1998. Iron-limited diatom growth and Si : N uptake ratios in a coastal upwelling regime. Nature 393, 561–564.

Jacquet, S.H.M., Dehairs, F., Dumont, I., Becquevort, S., Cavagna, a. J., Cardinal, D., 2011. Twilight zone organic carbon remineralization in the Polar Front Zone and Subantarctic Zone south of Tasmania. Deep. Res. Part II Top. Stud. Oceanogr. 58, 2222–2234. doi:10.1016/j.dsr2.2011.05.029

Jacquet, S.H.M., Dehairs, F., Elskens, M., Savoye, N., Cardinal, D., 2007. Barium cycling along WOCE SR3 line in the Southern Ocean. Mar. Chem. 106, 33–45. doi:10.1016/j.marchem.2006.06.007

Jacquet, S.H.M., Dehairs, F., Rintoul, S., 2004. A high resolution transect of dissolved barium in the Southern Ocean. Geophys. Res. Lett. 31, 7–10. doi:10.1029/2004GL020016

Jeandel, C., Dupré, B., Lebaron, G., Monnin, C., Minster, J.-F., 1996. Longitudinal distributions of dissolved barium, silica and alkalinity in the western and southern Indian Ocean. Deep Sea Res. Part I Oceanogr. Res. Pap. 43, 1–31. doi:10.1016/0967-0637(95)00098-4

Kim, I., Kim, G., Choy, E.J., 2015. The significant inputs of trace elements and rare earth elements from melting glaciers in Antarctic coastal waters 1, 1–13.

Klinkhammer, G.P., Chan, L.H., 1990. Determination of barium in marine waters by isotope dilution inductively coupled plasma mass spectrometry. Anal. Chim. Acta 232, 323–329.

Kozlowski, W.A., Deutschman, D., Garibotti, I., Trees, C., Vernet, M., 2011. An evaluation of the application of CHEMTAX to Antarctic coastal pigment data. Deep. Res. Part I Oceanogr. Res. Pap. 58, 350–364.

Lannuzel, D., Bowie, A.R., van der Merwe, P.C., Townsend, A.T., Schoemann, V., 2011. Distribution of dissolved and particulate metals in Antarctic sea ice. Mar. Chem. 124, 134–146. doi:10.1016/j.marchem.2011.01.004

LaVigne, M., Grottoli, A.G., Palardy, J.E., Sherrell, R.M., 2016. Multi-colony calibrations of coral Ba/Ca with a contemporaneous in situ seawater barium record. Geochim. Cosmochim. Acta. doi:10.1016/j.gca.2015.12.038

Lea, D., Boyle, E., 1989. Barium content of benthic foraminifera controlled by bottom-water composition. Nature 338, 751–753. doi:10.1038/338751a0

Lea, D.W., Spero, H.J., 1992. Experimental determination of barium uptake in shells of the planktonic foraminifera Orbulina universa at 22°C. Geochim. Cosmochim. Acta 56, 2673–2680. doi:10.1016/0016-7037(92)90352-J

Martin, J.-M., Meybeck, M., 1979. Elemental mass-balance of material carried by major world rivers. Mar. Chem. 7, 173–206. doi:10.1016/0304-4203(79)90039-2

Martinson, D.G., Stammerjohn, S.E., Iannuzzi, R. a., Smith, R.C., Vernet, M., 2008. Western Antarctic Peninsula physical oceanography and spatio–temporal variability. Deep Sea Res. Part II Top. Stud. Oceanogr. 55, 1964–1987. doi:10.1016/j.dsr2.2008.04.038

McManus, J., Berelson, W.M., Klinkhammer, G.P., Johnson, K.S., Coale, K.H., Anderson, R.F., Kumar, N., Burdige, D.J., Hammond, D.E., Brumsack, H.J., McCorkle, D.C., Rushdi, A., 1998. Geochemistry of barium

in marine sediments: implications for its use as a paleoproxy. Geochim. Cosmochim. Acta. doi:10.1016/S0016-7037(98)00248-8

McManus, J., Berelson, W.M., Klinkhammer, G.P., Kilgore, T.E., Hammond, D.E., 1994. Remobilization of barium in continental margin sediments. Geochim. Cosmochim. Acta 58, 4899–4907. doi:10.1016/0016-7037(94)90220-8

Meredith, M.P., Brandon, M. a., Wallace, M.I., Clarke, A., Leng, M.J., Renfrew, I. a., van Lipzig, N.P.M., King, J.C., 2008. Variability in the freshwater balance of northern Marguerite Bay, Antarctic Peninsula: Results from δ18O. Deep Sea Res. Part II Top. Stud. Oceanogr. 55, 309–322. doi:10.1016/j.dsr2.2007.11.005

Meredith, M.P., Stammerjohn, S.E., Venables, H.J., Ducklow, H.W., Martinson, D.G., Iannuzzi, R.A., Leng, M.J., van Wessem, J.M., Reijmer, C.H., Barrand, N.E., 2016. Changing distributions of sea-ice melt and meteoric water west of the Antarctic Peninsula. Deep Sea Res. Part II Top. Stud. Oceanogr.

Meredith, M.P., Venables, H.J., Clarke, A., Ducklow, H.W., Erickson, M., Leng, M.J., Lenaerts, J.T.M., van den Broeke, M.R., 2013. The Freshwater System West of the Antarctic Peninsula: Spatial and Temporal Changes. J. Clim. 26, 1669–1684. doi:10.1175/JCLI-D-12-00246.1

Meredith, M.P., Wallace, M.I., Stammerjohn, S.E., Renfrew, I. a., Clarke, A., Venables, H.J., Shoosmith, D.R., Souster, T., Leng, M.J., 2010. Changes in the freshwater composition of the upper ocean west of the Antarctic Peninsula during the first decade of the 21st century. Prog. Oceanogr. 87, 127–143. doi:10.1016/j.pocean.2010.09.019

Mitchell, A., Brown, G.H., Fuge, R., 2001. Minor and trace element export from a glacierized Alpine headwater catchment (Haut Glacier d'Arolla, Switzerland). Hydrol. Process. 15, 3499–3524. doi:10.1002/hyp.1041

Moline, M.A., Claustre, H., Frazer, T.K., Schofield, O., Vernet, M., 2004. Alteration of the food web along the Antarctic Peninsula in response to a regional warming trend. Glob. Chang. Biol. 10, 1973–1980.

Monnin, C., Cividini, D., 2006. The saturation state of the world's ocean with respect to (Ba,Sr)SO4 solid solutions. Geochim. Cosmochim. Acta 70, 3290–3298. doi:10.1016/j.gca.2006.04.002

Mora, S.J. De, Whitehead, R.F., Gregory, M., 1994. The chemical composition of glacial melt water ponds and streams on the McMurdo Ice Shelf, Antarctica. Antarct. Sci. 6, 17–27.

Nozaki, Y., Yamamoto, Y., Manaka, T., Amakawa, H., Snidvongs, A., 2001. Dissolved barium and radium isotopes in the Chao Phraya River estuarine mixing zone in Thailand. Cont. Shelf Res. 21, 1435–1448. doi:10.1016/S0278-4343(01)00023-1

Nürnberg, D., Wollenburg, I., Dethleff, D., Eicken, H., Kassens, H., Letzig, T., Reimnitz, E., Thiede, J., 1994. Sediments in Arctic sea ice: Implications for entrainment, transport and release. Mar. Geol. 119, 185–214. doi:10.1016/0025-3227(94)90181-3

Östlund, H.G., Hut, G., 1984. Arctic Ocean water mass balance from isotope data. J. Geophys. Res. Ocean. 89, 6373–6381. doi:10.1029/JC089iC04p06373

Paytan, A., Kastner, M., 1996. Benthic Ba fluxes in the central Equatorial Pacific, implications for the oceanic Ba cycle. Earth Planet. Sci. Lett. 142, 439–450. doi:10.1016/0012-821X(96)00120-3

Plewa, K., Meggers, H., Kasten, S., 2006. Barium in sediments off northwest Africa: A tracer for paleoproductivity or meltwater events? Paleoceanography 21, PA2015. doi:10.1029/2005PA001136

Raiswell, R., Benning, L.G., Tranter, M., Tulaczyk, S., 2008. Bioavailable iron in the Southern Ocean: the significance of the iceberg conveyor belt. Geochem. Trans. 9, 7.

Roeske, Tobias; Rutgers van der Loeff, Michiel M (2012): Barium measured on water bottle samples during POLARSTERN cruise ANT-XXIV/3. Alfred Wegener Institute, Helmholtz Center for Polar and Marine Research, Bremerhaven, doi:10.1594/PANGAEA.786619

Schenau, S.J., Prins, M. a., De Lange, G.J., Monnin, C., 2001. Barium accumulation in the Arabian Sea: Controls on barite preservation in marine sediments. Geochim. Cosmochim. Acta 65, 1545–1556. doi:10.1016/S0016-7037(01)00547-6

Schloss, I.R., Ferreyra, G.A., Ruiz-Pino, D., 2002. Phytoplankton biomass in Antarctic shelf zones: A conceptual model based on Potter Cove, King George Island. J. Mar. Syst. 36, 129–143.

Sherrell, R.M., Lagerström, M.E., Forsch, K.O., Stammerjohn, S.E., Yager, P.L., 2015. Dynamics of dissolved iron and other bioactive trace metals (Mn, Ni, Cu, Zn) in the Amundsen Sea Polynya, Antarctica. Elem. Sci. Anthr. 3, 000071.

Smith, K.L., Robison, B.H., Helly, J.J., Kaufmann, R.S., Ruhl, H. a, Shaw, T.J., Twining, B.S., Vernet, M., 2007. Free-drifting icebergs: hot spots of chemical and biological enrichment in the Weddell Sea. Science 317, 478–482. doi:10.1126/science.1142834

Sternberg, E., Tang, D., Ho, T.Y., Jeandel, C., Morel, F.M.M., 2005. Barium uptake and adsorption in diatoms. Geochim. Cosmochim. Acta 69, 2745–2752. doi:10.1016/j.gca.2004.11.026

Stroobants, N., Dehairs, F., Goeyens, L., Vanderheijden, N., Van Grieken, R., 1991. Barite formation in the Southern Ocean water column. Mar. Chem. 35, 411–421. doi:10.1016/S0304-4203(09)90033-0

Thomas, H., Shadwick, E., Dehairs, F., Lansard, B., Mucci, A., Navez, J., Gratton, Y., Prowe, F., Chierici, M., Fransson, A., Papakyriakou, T.N., Sternberg, E., Miller, L. a., Tremblay, J.-É., Monnin, C., 2011. Barium and carbon fluxes in the Canadian Arctic Archipelago. J. Geophys. Res. 116, C00G08. doi:10.1029/2011JC007120

Thompson, E.I., Schmitz, B., 1997. Barium and the late Paleocene d13C maximum : Evidence of increased marine surface productivity synchronous with the evolution of the late Paleocene in conjunction maximum versus water support originating. Paleoceanography 12, 239–254.

Timmermans, K.R., van der Wagt, B., 2010. VAriability in cell size, nutrient depletion, and growth rates of the

southern ocean diatom fragilariopsis kerguelensis (bacillariophyceae) after prolonged iron limitation. J. Phycol. 46, 497–506.

Tréguer, P.J., De La Rocha, C.L., 2013. The world ocean silica cycle. Ann. Rev. Mar. Sci. 5, 477–501.

Twining, B.S., Baines, S.B., 2013. The trace metal composition of marine phytoplankton. Ann. Rev. Mar. Sci. 5, 191–215.

Venables, H.J., Clarke, A., Meredith, M.P., 2013. Wintertime controls on summer stratification and productivity at the western Antarctic Peninsula. Limnol. Oceanogr. 58, 1035–1047. doi:10.4319/lo.2013.58.3.1035

Viers, J., Dupré, B., Gaillardet, J., 2009. Chemical composition of suspended sediments in World Rivers: New insights from a new database. Sci. Total Environ. 407, 853–868. doi:10.1016/j.scitotenv.2008.09.053

Von Damm, K.L., Edmond, J.M., Grant, B., Measures, C.I., 1985. Chemistry of submarine hydrothermal solutions at 21°N, East Pacific Rise. Geochim. Cosmochim. Acta 49, 2197–2220. doi:http://dx.doi.org/10.1016/0016-7037(85)90222-4

Wolgemuth, K., Broecker, W.S., 1970. Barium in sea water. Earth Planet. Sci. Lett. 8, 372–378. doi:10.1016/0012-821X(70)90110-X

Captions for main text Fig.s and tables:

Fig. 1 - Map showing the Palmer Long Term Ecological Research grid (PalLTER) covering waters adjacent to the West Antarctic Peninsula. Black circles and crosses indicate surface sample sites from cruises LMG11-01 (02/01/2011 – 06/02/2011) and LMG12-01 (30/12/2011 – 07/02/2012): red filled circles represent stations occupied in both years, crosses/open circles stations occupied only in 2011/2012 respectively. Location of two depth profiles at grid stations 200.100 and 200.160 in 2012 shown by filled black squares. Grid lines are labelled from -100 to 600, stations denoted by grid line plus approximate kilometres from the base tangent of the grid (e.g. 200.100 – station 100km along grid line 200). Grey squares indicate the location of Palmer Station on Anvers Island and the Rothera Station on Adelaide Island.

Fig. 2 – Surface distributions across the PalLTER: a. Dissolved barium concentrations (Ba_d, nM) in 2011; b. Dissolved barium concentrations (Ba_d, nM) in 2012; c. Silicic acid concentrations (μM) in 2011, dotted line shows the division between the continental shelf and slope, after Martinson et al. 2008, MB - Marguerite Bay; d. Silicic acid concentrations (μM) in 2012; e. and f. Barium residual values ($Ba_{Si}^{Residual} = Ba_d^{measured} – ((Si(OH)_4^{measured} * 0.21) + 69.2))$) for 2011 and 2012 respectively.

Fig. 3 - a. Depth profiles of dissolved Ba (nM) at PalLTER station 200.100 (filled circles) and station 200.160 (filled squares), horizontal error bars set at 1% to reflect the most conservative reproducibility of Ba determination in comparable seawater standards across these analytical runs. Depth profiles of dissolved barium from the Drake Passage from Roeske and Rutgers van der Loeff (2012), PS71/230-3 (open triangles) [lat -60.1077°N long -55.2821°E] and PS71/236-3 (open diamonds) [lat -58.9704°N long-58.1388°E], horizontal error bars within symbol size. b. Depth profiles of silicic acid (µM) at PalLTER station 200.100 (filled circles) and station 200.160 (filled squares).

Fig. 4 – a. Scatter plot of ΔBa against $\Delta Si(OH)_4$, indicating difference in these variables between 2011 and 2012 on a station by station basis. Zero lines are shown for reference. Dotted line indicates the linear regression model fit to all data (r^2=0.462; p=4.9*10^{-5}; $\Delta Si(OH)_4$ co-efficient=0.196; n=29); b. Scatter plot of ΔBa against the Δ%SI , indicating difference in these variables between 2011 and 2012. Dotted line indicates the linear regression model fitted to all data (r^2=0.316; p=0.0012; Δ%SI co-efficient=-1.75; n=30).

Fig. 5 - Dissolved barium (nM) vs. silicic acid (µM) for seawater samples across the PalLTER grid. Filled circles represent surface samples from 2011; open circles represent surface samples from 2012; crosses represent depth samples from 2012. Dotted line indicates the linear regression model fit to all of these samples (r^2=0.71; p=2.9*10^{-33}; $Si(OH)_4$ co-efficient=0.210; n=117). Ba errors shown are set to 2%, which is the most conservative estimate of uncertainty assessed using the long term external reproducibility of two comparable seawater standards (see Table 1).

Fig. 6 – Surface distributions of freshwater mass fractions (as calculated in section 2.3) across the PalLTER. Meteoric water and sea-ice melt fractions are presented as percentages, with a systematic error of ±1% on all absolute values. a. Fraction of meteoric water (%MW) in 2011; b. Fraction of meteoric water (%MW) in 2012; c. Fraction of sea-ice meltwater (%SI) in 2011; d. Fraction of sea-ice meltwater (%SI) in 2012.

Fig. 7 – Dissolved barium (Ba_d) (nM) vs. salinity across the PalLTER surface samples. Filled light grey circles represent shelf stations; filled dark grey squares represent off-shelf stations. Ba errors shown are set to 2%, which is the most conservative estimate of uncertainty assessed using two comparable seawater standards (see Table 1).

Fig. 8 – Dissolved barium (Ba_d) (nM) vs. meteoric water fraction, determined via oxygen isotopes, across the PalLTER in surface samples. Filled light grey circles represent shelf stations; filled dark grey squares represent off-shelf stations, un-filled squares represent off-shelf stations from 000 and -100 lines. Dotted lines indicate

the linear regression model fit to all of these samples (2011: r^2=0.23; p=0.0017; %MW co-efficient=2.29; n=41. 2012: r^2=0.097; p=0.024; %MW co-efficient=1.19; n=52). Ba errors shown are set to 2%, which is the most conservative estimate of uncertainty assessed using two comparable seawater standards (see Table 1). Uncertainty on the meteoric water fraction is ±1%, but this is not displayed as the majority of the error can be attributed to uncertainty on end-member values, and is therefore be systematic across the dataset and should not affect the significance of the linear regression model.

Fig. 9 – a. $Ba_{Si}^{residual}$ vs. fraction of sea-ice melt (%) for 2012 surface data. Dotted line indicates the linear regression model fitted to all data (r^2=0.235; p=0.00026; SI% co-efficient=-0.92; n=52); b. Scatter plot of $Ba_{Si}^{residual}$ against salinity for 2012 surface data. Dotted line indicates the linear regression model fit to all data (r^2=0.154; p=0.004; n=52). Uncertainty on the sea-ice melt fraction is ±1%, but this is not displayed as the majority of the error can be attributed to uncertainty on end-member values, and is therefore be systematic across the dataset and should not affect the significance of the linear regression model.

Table 1 - Reproducibility of standards in the Rutgers and Cardiff University laboratories where samples were measured. Values given are 2*relative standard deviation (2*RSD). Errors from In-house Standard 1 and 2 (from the Southern Ocean and Amundsen Sea respectively) are considered applicable to PalLTER samples, as the average dissolved barium concentrations are the most comparable.

Table 2 – Linear regression models applied to Ba_d-$Si(OH)_4$ in Antarctic adjacent waters. All studies included both depth and surface samples, excepting entry for 'WAP surface' which includes only surface samples from this study.

Table 3 – Multiple regression analysis (r^2 of model =0.631; significance f of model =$1.3*10^{-5}$) of the inter-year variance (2012-2011), with three independent variables: $\Delta Si(OH)_4$, Δ%MW, and Δ%SI, predicting the inter-year variance in the dissolved barium distribution.

Supplementary Fig. captions:

Supplementary Fig. 1 – Map showing the location of depth profiles used to compare variation in Ba_d concentration with depth on and off the continental shelf. Stations 200.100 and 200.160 are part of the PalLTER dataset analysed for this study, collected in austral summer 2012. PS71/236 and PS71/230 are from Roeske and van der Loeff (2012) collected in austral autumn 2008 (PS71/236 collected on 05/04/2008 [lat -58.9704°N long-58.1388°E]; PS71/230 collected on 02/04/2008 [lat -60.1077°N long -55.2821°E]).

Supplementary Fig. 2 – Surface distributions across the PalLTER for 2011 (left hand column) and 2012 (right hand column): a. Nitrate plus nitrite concentrations (NOx) (µM); b. Phosphate concentrations (PO_4) (µM); c. Salinity; d. Temperature (°C).

Supplementary Fig. 3 - a. Sea-ice melt fraction (%) vs. silicic acid (µM) for 2011 and 2012, showing no correlation between the variables (2011: r2=0.05, p=0.18, n=40; 2012: r2=0.07, p=0.064, n=52); b. Sea-ice melt fraction (%) vs. dissolved barium (nM) for 2011 and 2012, showing no correlation between the variables (2011: r2=0.01, p=0.57, n=41; 2012: r2=0.03, p=0.21, n=52). Ba errors shown are set to 2%, which is the most conservative estimate of uncertainty assessed using two comparable seawater standards (see Table 1). Freshwater fraction errors are not displayed, as the majority of the 1% error on absolute values can be attributed to uncertainty on end-member values, and will therefore be systematic across the dataset.

Supplementary Fig. 4 – Surface plots showing values for primary production (mg/m³/day) at selected stations in the PalLTER grid. Colour scale from purple (lowest values) – blue – green – yellow – orange – red – pink (highest values); a. 2011; b. 2012.

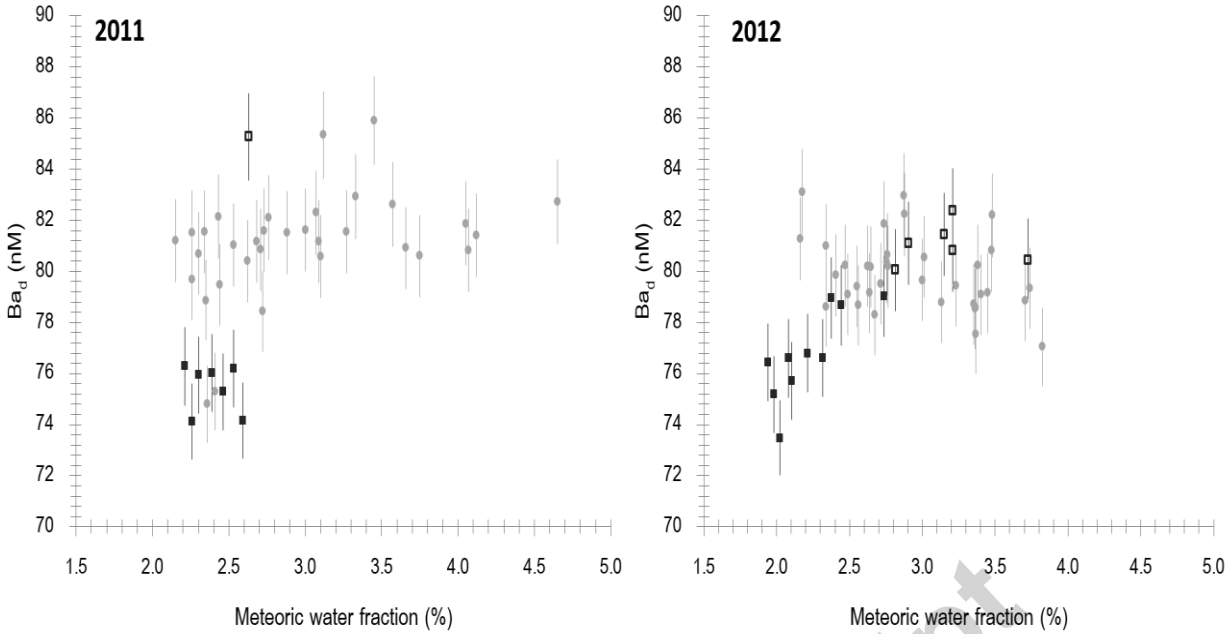

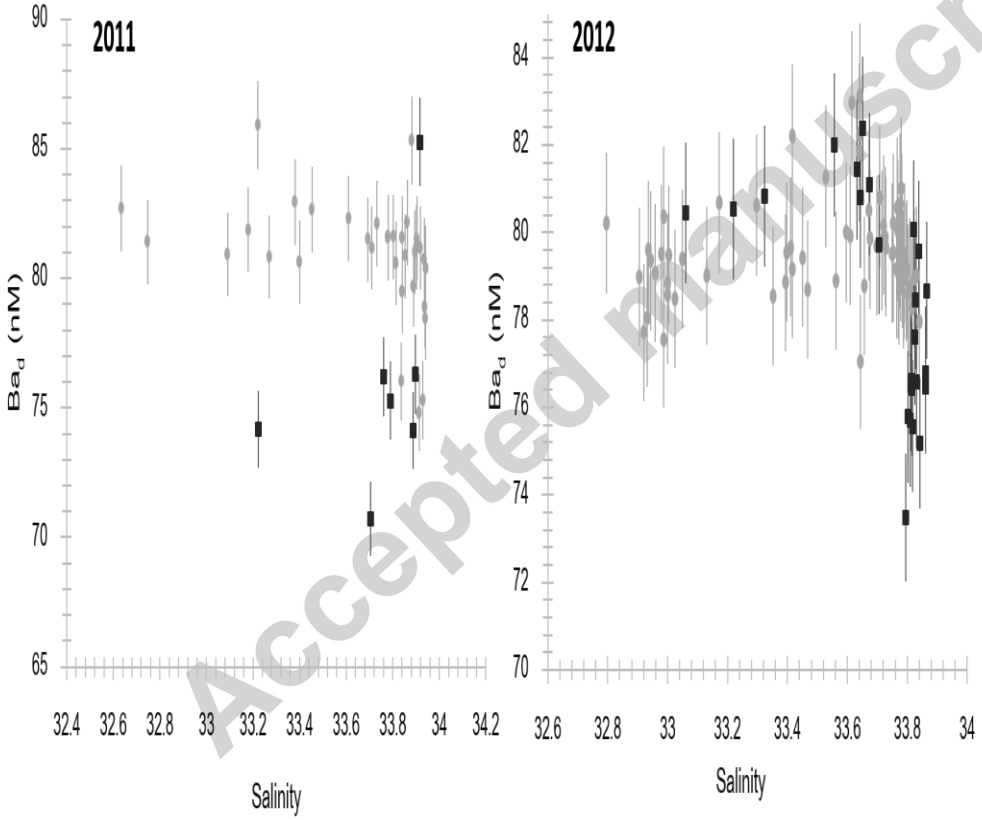

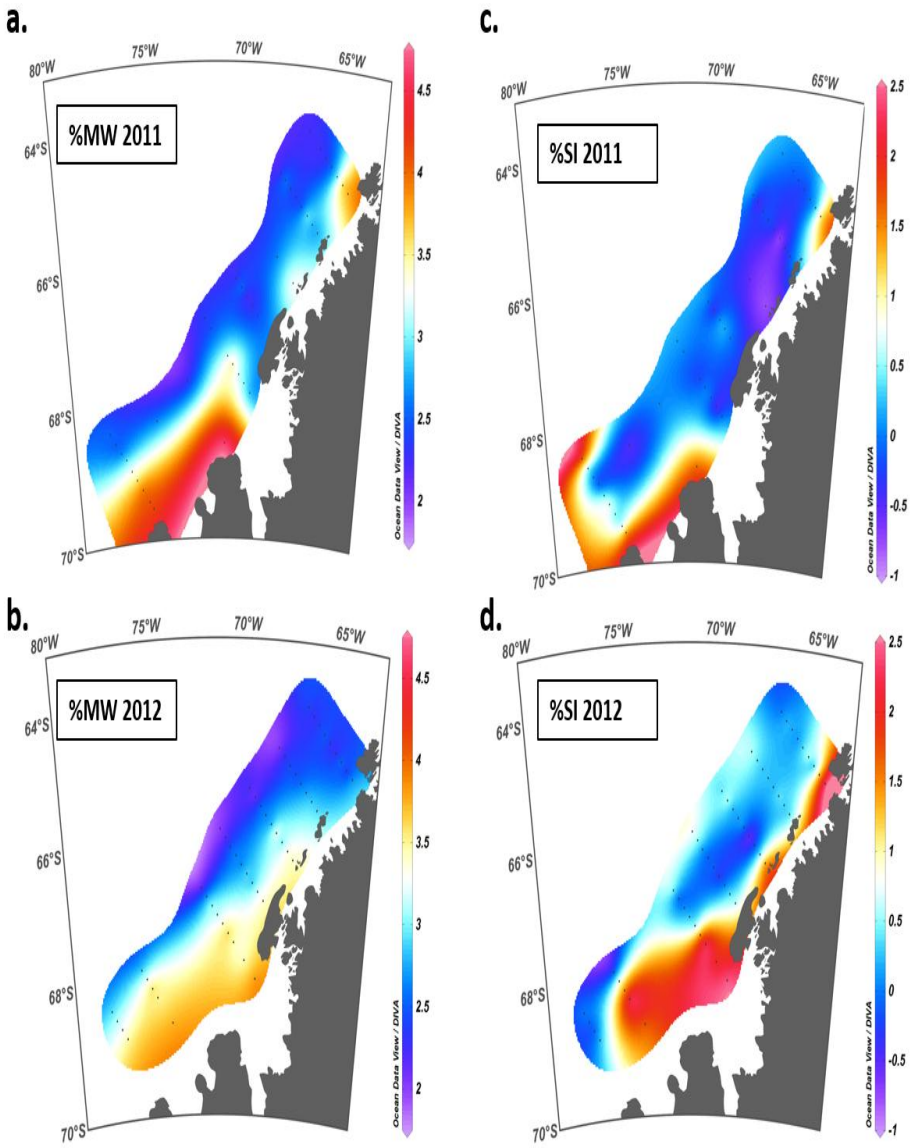

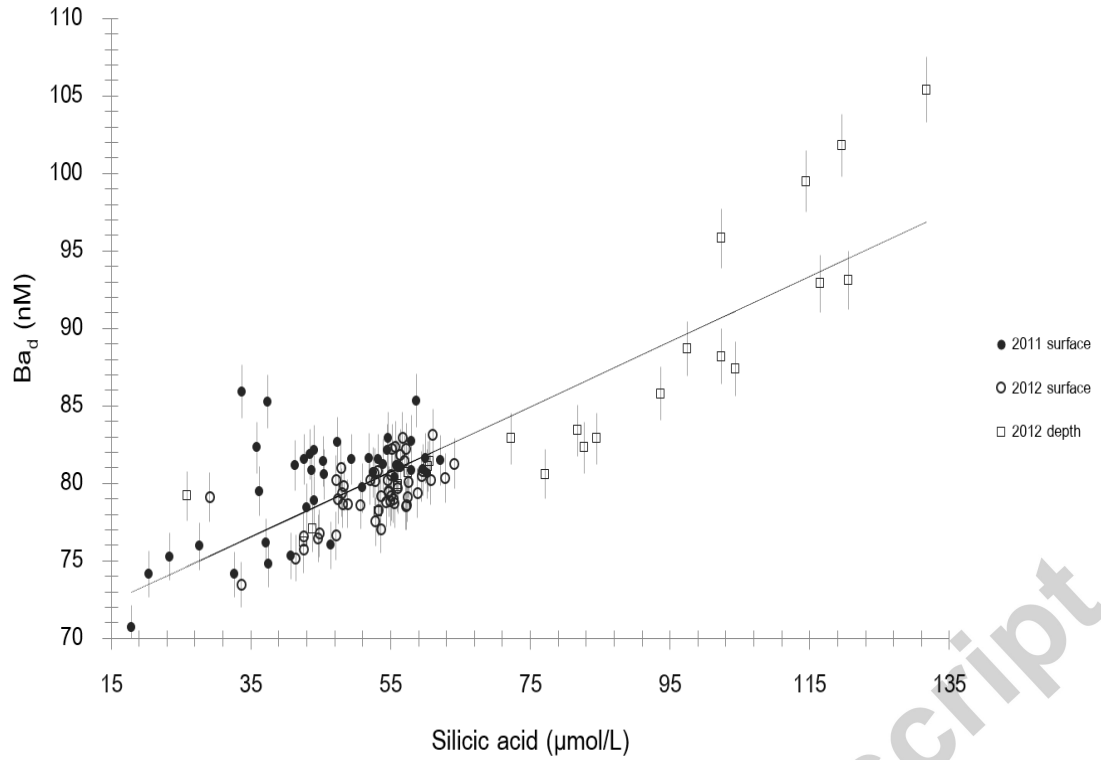

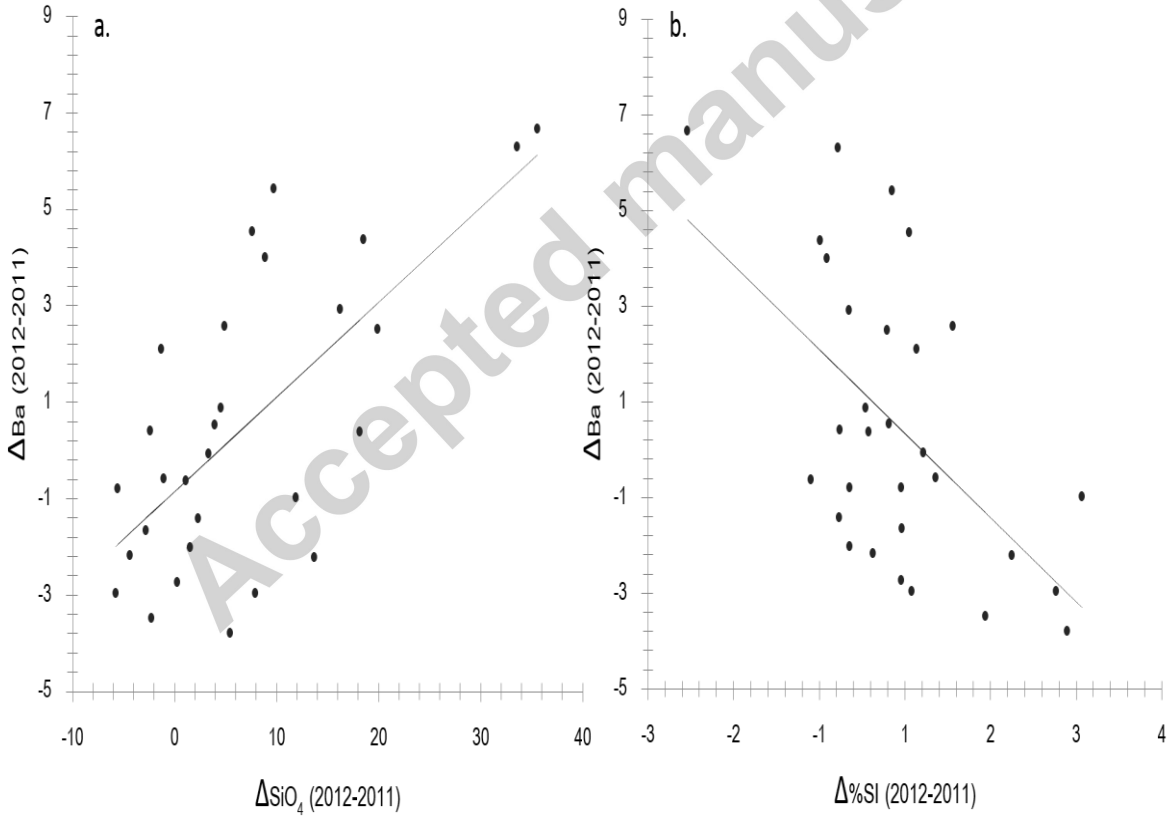

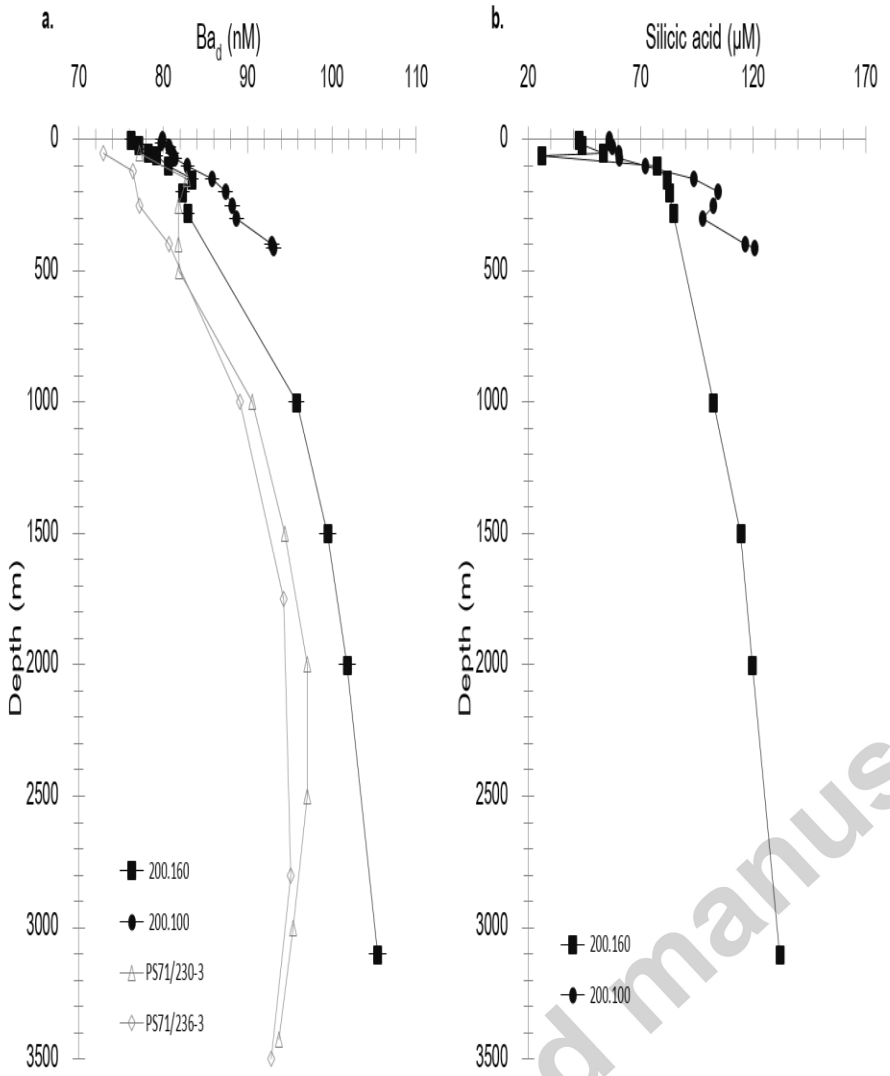

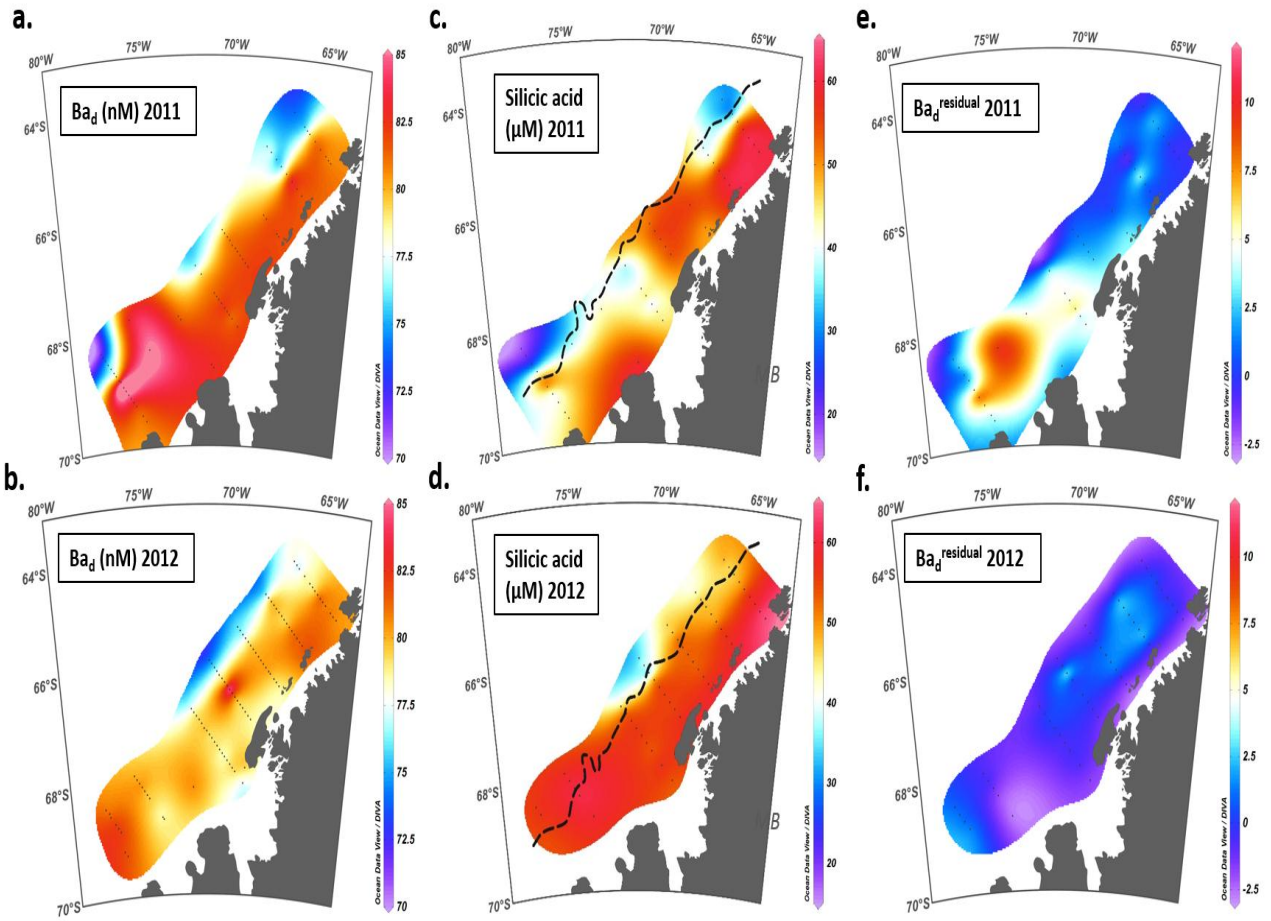
a.
Ba$_d$ (nM) 2011
b.
Ba$_d$ (nM) 2012
c.
Silicic acid (µM) 2011
d.
Silicic acid (µM) 2012
e.
Ba$_d^{residual}$ 2011
f.
Ba$_d^{residual}$ 2012
80°W
75°W
70°W
65°W
64°S
66°S
68°S
70°S
Ocean Data View / DIVA

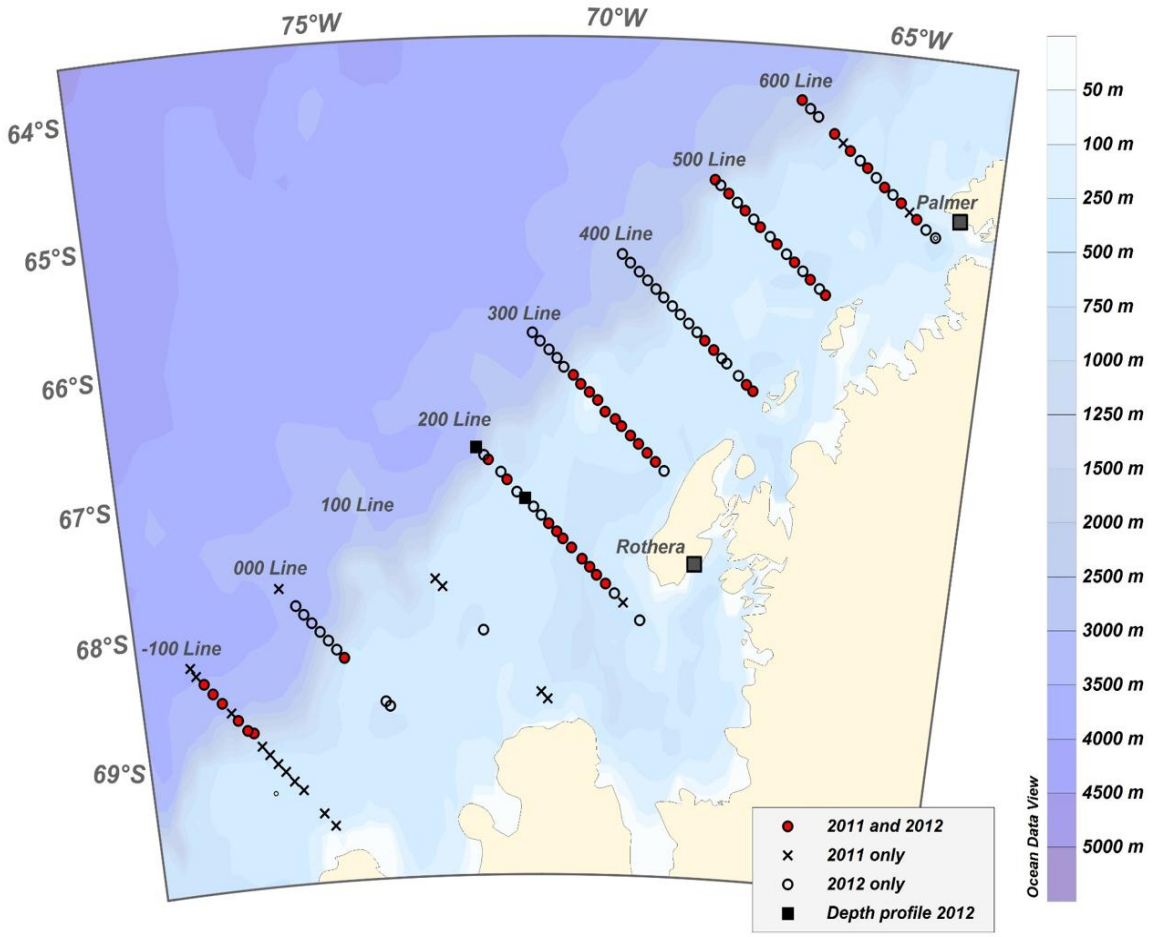
75°W
70°W
65°W
64°S
65°S
66°S
67°S
68°S
69°S
600 Line
500 Line
400 Line
300 Line
200 Line
100 Line
000 Line
-100 Line
Palmer
Rothera
2011 and 2012
2011 only
2012 only
Depth profile 2012
Ocean Data View
50 m
100 m
250 m
500 m
750 m
1000 m
1250 m
1500 m
2000 m
2500 m
3000 m
3500 m
4000 m
4500 m
5000 m

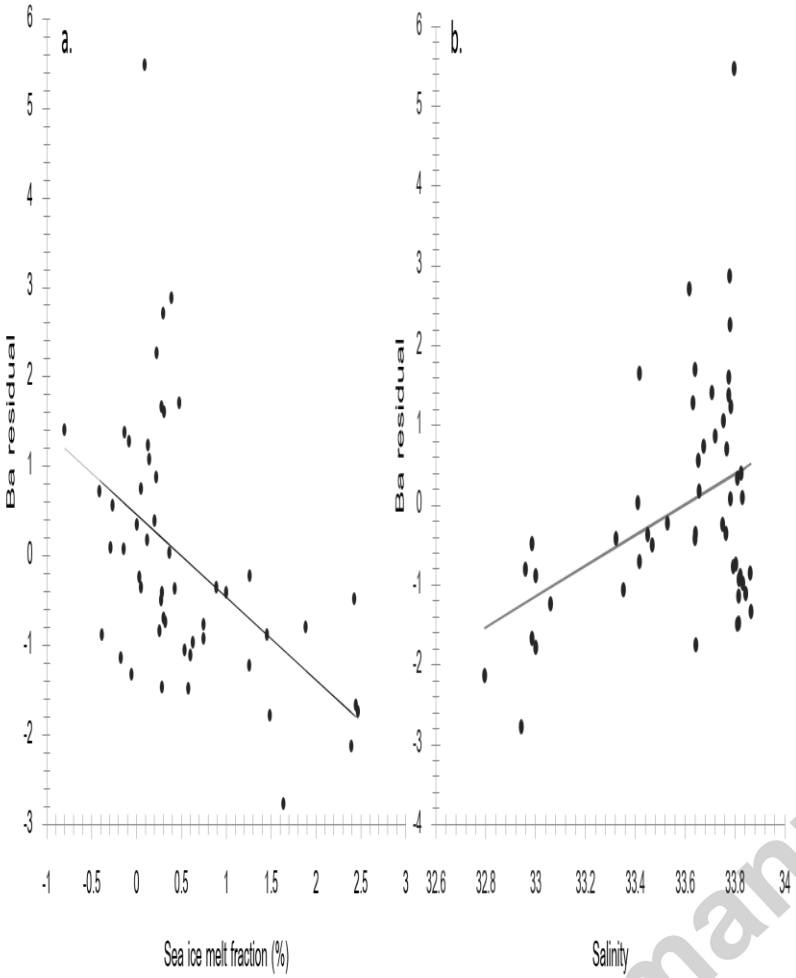

Tables:

Table 1:

Standard:		In-house Standard 1	In-house Standard 2	NASS-5	NASS-6
Rutgers	2*RSD	1.63%	2.07%	2.46%	2.84%
	n	27	27	27	26
	Average [Ba](nM)	74.1	83.2	37.1	49.7
Cardiff	2*RSD	1.29%	1.76%	1.53%	1.22%
	n	23	23	22	23

	Average [Ba] (nM)	73.7	83.8	37.0	49.5

Table 2:

Location	Slope co-efficient	Intercept at zero SiO_4	R^2	p-value	Reference
N. Indian Ocean	0.56	38.2	-	-	Jeandal et al. 1996
S. Indian Ocean	0.25	64.5	-	-	Jeandal et al. 1996
145°E PFZ-AZ	0.23±0.01	64.1±0.7	0.72	<0.001	Jacquet et al. 2007
145°E SAF-PFZ	0.31±0.01	58.7±0.8	0.91	<0.001	Jacquet et al. 2007
Prime Meridian	0.2645	59.368	0.909	-	Hopemma et al. 2010
Weddell Sea	0.2322	66.227	0.806	-	Hoppema et al. 2010
WAP all	0.21	69.2	0.716	<0.001	This study
WAP surface	0.14	72.8	0.266	<0.001	This study

Table 3:

	Co-efficients	Standard Error	t Stat	P-value
Intercept	-0.034	0.503	-0.0675	0.946
ΔSiO_4	0.17	0.0379	4.61	0.0001
Δ%MW	-0.84	0.716	-1.17	0.252

Δ%SI	-1.3	0.398	-3.28	0.003